Monitoring Committee Progress Report #4

Numerical Representation of Mountains in Atmospheric Models

James Shaw

Supervisors: Hilary Weller, John Methven, Terry Davies

Monitoring Committee: Paul Williams, Maarten Ambaum

24th November 2016

1 Introduction

An atmospheric model solves the equations of motion in discrete form on a numerical mesh. This mesh becomes distorted over sloping terrain, and the distortions can result in numerical errors. With new atmospheric models using increasingly fine mesh spacing, steep slopes become resolved by the mesh. These steep slopes can result in highly-distorted meshes that can lead to larger numerical errors. My PhD project seeks out new techniques for reducing numerical errors in regions of steep terrain.

There are several methods for representing terrain on a mesh. Operational models use some form of terrain-following transformation that distorts horizontal mesh layers to accommodate the terrain. Such meshes are straightforward to represent using a uniform rectangular computational mesh, but sloped terrain distorts the mesh far above the surface, leading to larger errors (Schär et al., 2002; Klemp, 2011). The cut cell method is an alternative to terrain-following transformations in which a piecewise linear representation of the surface is intersected with a uniform rectangular mesh. Cut cell meshes are less distorted than terrain-following meshes, but the cut cell method creates arbitrarily small cells that impose severe timestep constraints on explicit numerical methods (Klein et al., 2009). Other representations of terrain have also been used, such as the sloping step method used in the Eta model (Mesinger et al., 2012) and unstructured tetrahedral meshes (Smolarkiewicz and Szmelter, 2011).

The wide variety of mesh types motivates the development of finite volume methods for arbitrary meshes. This enables a like-for-like comparison between different types of mesh and allows us to assess the characteristics of new types of mesh. Further, we hope that the new methods we develop will be less sensitive to mesh distortions compared to traditional methods.

My project comprises three parts. First, a new type of mesh called the slanted cell mesh has been developed that is less distorted than terrain-following meshes and avoids arbitrarily small cells that are associated with the cut cell method (Shaw and Weller, 2016). Second, we have designed an explicit, Eulerian transport scheme that is accurate near highly-distorted lower boundaries and is suitable for a variety of mesh types. Third, we intend to generalise the Charney–Phillips staggering for arbitrary meshes and hope that this new formulation will alleviate the computational mode that is associated with the Lorenz staggering of variables (Arakawa and Konor, 1996).

2 A new finite volume scheme for transport over steep slopes

In May 2016, monitoring committee report #3 (hereafter MC3) described our progress developing an explicit, Eulerian transport scheme which has been named “cubicFit”. At that time the scheme was numerically unstable on some meshes. We have since improved stability using additional constraints derived from a von Neumann analysis. No further stability problems have been encountered since the

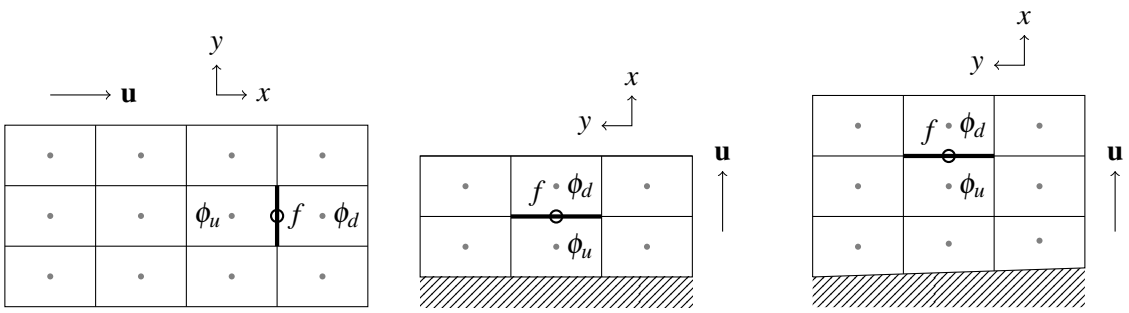

(a) 12-point stencil for a face in the interior of a two-dimensional quadrilateral mesh

(b) 6-point stencil for a face near a flat lower boundary

(c) 9-point stencil for a face near a sloping lower boundary. When the slope is only slight then there is insufficient variation in x to fit the x^3 polynomial term.

Figure 1: Example stencils for different regions of quadrilateral meshes. The wind direction $\mathbf{u}$ and local x–y coordinate system is indicated for each stencil. The origin of the local coordinate system is positioned at the centroid of face f marked by an open circle. Cell centres are marked by grey dots. The values of the dependent variable ϕ immediately upwind and downwind of face f are labelled ϕ_u and ϕ_d respectively.

improvement was implemented. In this section, an overview of the cubicFit scheme is provided, and some details of the von Neumann stability analysis are outlined.

The discretisation starts from the flux form transport equation of a dependent variable ϕ,

$$\frac{\partial \phi}{\partial t} - \nabla \cdot (\mathbf{u}\phi) = 0 \tag{1}$$

where $\mathbf{u}$ is the wind field. A C-grid staggering is used such that the dependent variable ϕ is prognosed at cell centroids and the wind is prescribed at face centroids. The divergence term in equation (1) is discretised using Gauss' divergence theorem,

$$\nabla \cdot (\mathbf{u}\phi) \approx \sum_{f \in c} \mathbf{u}_f \cdot \mathbf{S}_f \phi_F \tag{2}$$

where $\sum_{f \in c}$ denotes a summation over faces f of cell c, $\mathbf{u}_f$ is the wind vector prescribed at the face, and $\mathbf{S}_f$ is the vector that is outward normal to the face having a magnitude equal to the face area. ϕ_F is an approximation of the dependent variable at the face centroid. The accuracy of this approximation is crucial to the accuracy of the transport scheme.

The cubicFit scheme approximates the value ϕ_F by fitting a multidimensional polynomial over a stencil of cell centre values using a least-squares approach. An example stencil for a face in the interior of a two-dimensional quadrilateral mesh is shown in figure 1a. The polynomial for such a face is

$$\phi = a_1 + a_2 x + a_3 y + a_4 x^2 + a_5 xy + a_6 y^2 + a_7 x^3 + a_8 x^2 y + a_9 xy^2 \tag{3}$$

By choosing a local coordinate with its origin positioned at the face centroid then $\phi_F = a_1$. The value of ϕ_F is calculated as a weighted sum of cell centre values,

$$\phi_F = \begin{bmatrix} w_u \\ w_d \\ w_3 \\ \vdots \\ w_n \end{bmatrix} \cdot \begin{bmatrix} \phi_u \\ \phi_d \\ \phi_3 \\ \vdots \\ \phi_n \end{bmatrix} = \mathbf{w} \cdot \boldsymbol{\phi} \tag{4}$$

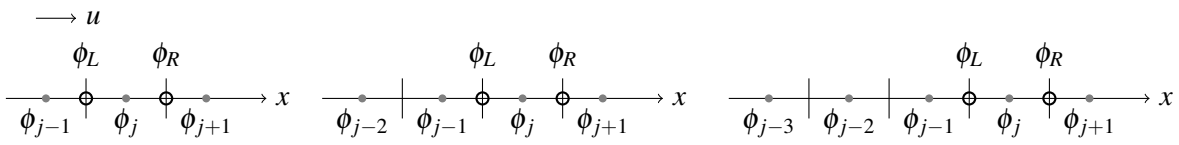

(a) 2-point approximation (b) 3-point approximation (c) 4-point approximation

Figure 2: Schematics of one-dimensional linear transport discretisations with uniform wind and constant mesh spacing. The von Neumann analysis starts with the 2-point approximation and subsequent analyses introduce additional points. The 4-point approximation is constructed to mimic the configuration of typical stencils used by cubicFit, such as the stencil in figure 1a. Cell centres are marked by grey filled circles and faces are marked by black open circles. The uniform wind u is from left to right.

where n is the number of cells in the stencil for face f. By convention the upwind cell is the first component and the downwind cell is the second component.

For stencils near boundaries (figure 1b) and for stencils in some distorted mesh regions (figure 1c), there is insufficient information to fit all nine polynomial terms in equation (3). We can detect such cases by checking whether the matrix equation that results from the least squares procedure is numerically full rank (details are provided in MC3).

For stencils in some other distorted mesh regions, there is sufficient information to fit equation (3), but the resulting weights lead to an unstable transport scheme. To detect these cases, we evaluate the weights vector $\mathbf{w}$ against a set of constraints that are derived from a von Neumann stability analysis.

Von Neumann stability analysis

The analysis starts by considering the one-dimensional linear transport equation that is continuous in time and discretised in space,

$$\frac{\partial \phi_j^{(n)}}{\partial t} = -u\frac{\phi_R - \phi_L}{\Delta x} \tag{5}$$

with left- and right-hand face approximations, ϕ_L and ϕ_R, separated by mesh spacing Δx (figure 2a). The face approximations are calculated as weighted sums of the neighbouring cell centre values,

$$\phi_L = w_u\phi_{j-1} + w_d\phi_j \tag{6}$$

$$\phi_R = w_u\phi_j + w_d\phi_{j+1} \tag{7}$$

where we assume that the upwind weight w_u and downwind weight w_d are the same for both left- and right-hand faces. We replace ϕ with the Fourier decomposition

$$\phi_j^{(n)} = A^n e^{ijk\Delta x} \tag{8}$$

where $\phi_j^{(n)}$ denotes the value of ϕ at position $j\Delta x$ and time level (n), and k is a wavenumber. The wind u is taken to be positive. The amplification factor A is constrained such that $|A| \leq 1$ and $\arg(A) < 0$ so that the solution has a physical phase speed and does not amplify. Additionally, A must be no less than the amplification factor for a first-order upwind scheme (in which $w_u = 1$, $w_d = 0$). Similar analyses are performed for three-point approximations (figure 2b) and four-point approximations (figure 2c) to obtain the constraints on $\mathbf{w}$,

$$0.5 \leq w_u \leq 1 \tag{9}$$

$$0 \leq w_d \leq 0.5 \tag{10}$$

$$w_u - w_d \geq \max_{p \in P}(|w_p|) \tag{11}$$

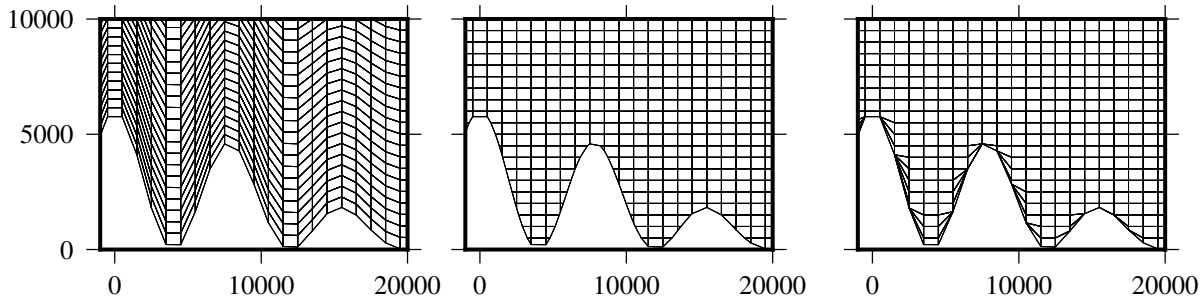

(a) Basic terrain-following mesh (b) Cut cell mesh (c) Slanted cell mesh

Figure 3: The edges of the three meshes used in the two-dimensional tracer transport test. The same wave-shaped mountain is represented by all three meshes. The mesh spacing is $\Delta x = 1000\,\text{m}$ and $\Delta z = 500\,\text{m}$. The peak mountain height is 6 km. Only part domain near the mountain is shown. The entire domain is 301 km wide and 25 km high.

where P are the peripheral cells $\{w_3, \ldots, w_n\}$.

The full-rank constraint and von Neumann stability constraints are used to select the most suitable subset of polynomial terms from equation (3) (the subset includes the set itself). The monitoring committee raised a concern about this procedure in our third meeting: which terms should be retained and which should be discarded? Recent improvements address this issue. We generate a set of candidate polynomials and select the candidate with the greatest number of terms that satisifies all constraints. Candidate polynomials are generated such that high-order terms are discarded first. More precisely, let

$$M(x,y) = x^i y^j : i, j \geq 0 \text{ and } i + j \leq 3 \tag{12}$$

be the set of all monomials of degree at most 3 in x, y. A subset S of $M(x,y)$ is "dense" if, whenever $x^a y^b$ and $x^c y^d$ are in S with $a \leq c$ and $b \leq d$, then $x^i y^j$ is also in S for all $a < i < c$, $b < j < d$. The candidate polynomials are all the dense subsets of $M(x,y)$. If multiple candidates with the same number of terms satisfy the constraints, the candidate with the best-conditioned matrix is chosen.

A new tracer transport test over steep terrain

In MC3 we presented preliminary results of two-dimensional test case that used transported a stably-stratified thermal profile in a terrain-following wind field over orography. We have since replaced this test with a variation of the standard orographic transport test by Schär et al. (2002). Test results are compared on a basic terrain-following (BTF) mesh (figure 3a), cut cell mesh (figure 3b), and slanted cell mesh (figure 3c). Three modifications were made to the standard test:

1. The peak mountain height was raised to 6 km in order to present a greater challenge to the cubicFit scheme.

2. A terrain-following wind field was prescribed that is misaligned with all three meshes. This was done to ensure that flow crosses mesh layers in all tests.

3. The tracer was centred at the ground in order to assess transport accuracy over the lower boundary.

Figure 4 shows the evolution of the tracer with snapshots plotted at the initial time $t = 0\,\text{s}$, half-way time $t = 5000\,\text{s}$, and end time $t = 10\,000\,\text{s}$. At $t = 5000\,\text{s}$ the tracer is positioned above the mountain and has been distorted by the terrain-following winds. Once the tracer clears the mountain the analytic solution returns to its original shape (shown by dotted contours in figure 4). The numerical result plotted with solid contours in figure 4 was obtained on the basic terrain-following mesh using the cubicFit scheme. Slight distortions are apparent at $t = 10\,000\,\text{s}$ compared to the analytic solution.

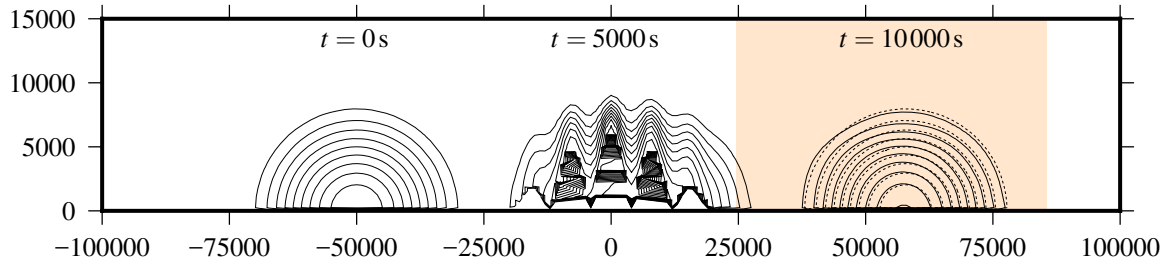

Figure 4: Evolution of the tracer in the two-dimensional transport test over steep terrain. The tracer is transported to the right over the wave-shaped terrain. Tracer contours are every $0.1\,\mathrm{kg\,m^{-3}}$. The result obtained using the cubicFit scheme on the basic terrain-following mesh is shown at $t = 0\,\mathrm{s}$, $t = 5000\,\mathrm{s}$ and $t = 10000\,\mathrm{s}$ with solid black contours. The analytic solution at $t = 10000\,\mathrm{s}$ is shown with dotted contours. The shaded box indicates the region that is plotted in figure 5. TODO: *try to mask off below the mountain to hide the messy contouring*

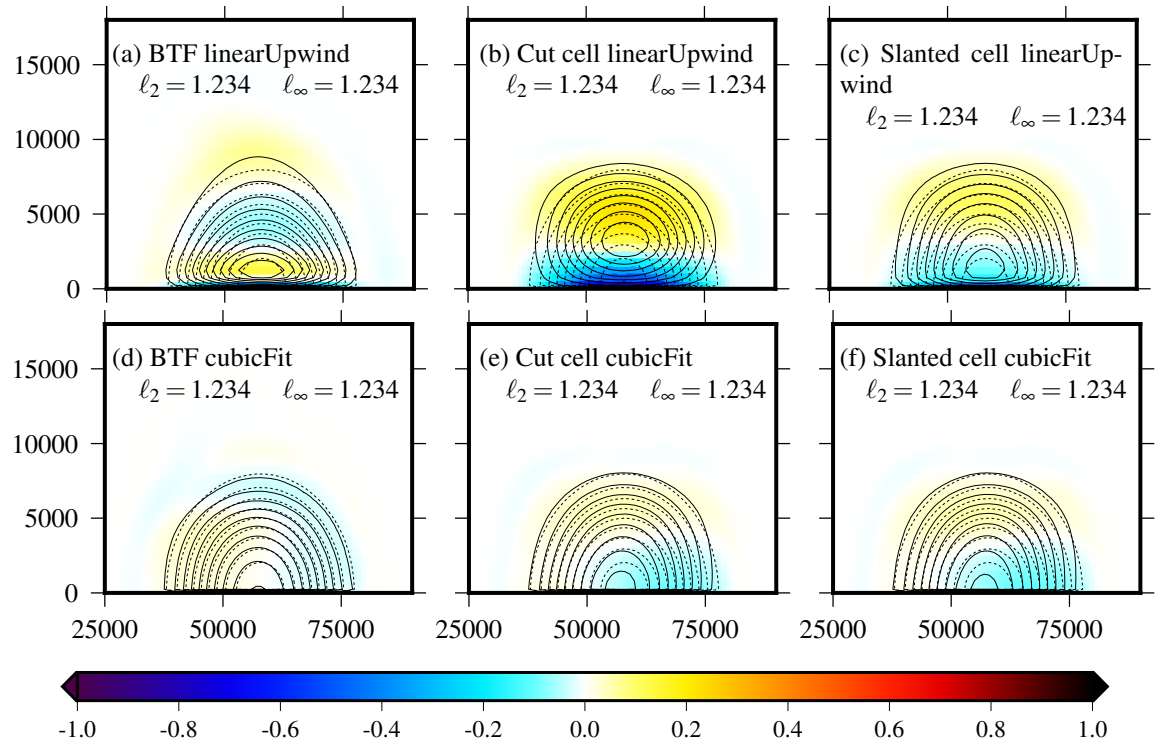

Figure 5: Tracer contours at $t = 10000\,\mathrm{s}$ for the two-dimensional tracer transport tests. A region in the lee of the mountain is plotted corresponding to the shaded area in figure 4. Results are presented on BTF, cut cell and slanted cell meshes (shown in figure 3) using the linearUpwind and cubicFit transport schemes. The numerical solutions are marked by solid black lines. The analytic solution is marked by dotted lines. Contours are every $0.1\,\mathrm{kg\,m^{-3}}$. The error field is shaded in colour.

To assess the accuracy of cubicFit, results are compared against a standard linearUpwind scheme (OpenFOAM user guide). Numerical solutions are presented using solid contours in figure 5. The analytic solutions are shown with dotted contours and the error field is shaded in colour. Errors are largest using the linearUpwind scheme on the cut cell mesh. Results are improved using the linearUpwind scheme with slanted cell mesh or basic terrain-following mesh. A great improvement is found using the cubicFit scheme, which is seen to be largely insensitive to the choice of mesh.

We expect that few or no further modifications to the transport scheme will be needed. Since our meeting in May 2016, we realised that further experiments were needed to demonstrate that the cubicFit scheme is suitable for non-quadrilateral meshes. To address this, we have performed tests on a sphere using standard deformational flow tests by Lauritzen et al. (2012) on hexagonal icosahedra. Work is now underway to document the cubicFit scheme and experimental results. We intend to submit a manuscript to the Journal of Computational Physics in early 2017.

3 Future research

Work has progressed well since the previous meeting in May 2016, though an additional 1–2 months was taken with additional transport tests on the sphere. Here we present a revised timeline of tasks:

January 2017 Submit a manuscript documenting the cubicFit transport scheme to the Journal of Computational Physics.

February 2017 Begin work on generalising the Charney–Phillips staggering for arbitrary meshes. Start by verifying that existing test cases, such as those from Arakawa and Konor (1996), are able to excite the Lorenz computational mode using the nonhydrostatic model by Weller and Shahrokhi (2014).

April 2017 Complete modifications to the nonhydrostatic model to enable execution using the generalised Charney–Phillips staggering. The model should include a simple transport scheme for potential temperature. The model will have a fully-explicit formulation.

Summer 2017 Time permitting, the model should be improved using a more accurate transport scheme. Such a scheme will likely be based on the cubicFit scheme that we have already implemented. The model might also be extended with a semi-implicit treatment of gravity waves.

Autumn 2017 Complete main thesis chapters (outlined in Appendix A) including all test results.

Early 2018 Complete PhD.

4 Personal development

This section highlights some of my recent personal developments. A complete training record is available in the appendix.

I hope to attend two conferences next year. Hilary recommended PDEs on the Sphere as an excellent venue to present my work to an audience of numerical geoscientists. I would also like to attend SciCADE, a conference on Scientific Computation and Differential Equations, in order to meet numerical scientists and mathematicians working in other disciplines.

I have gained more experience as a reviewer, having provided feedback on the MSc dissertation of Hilary's most recent MSc student, Christiana Skea. We were extremely pleased that Christiana was awarded the MSc dissertation prize for her work. I have also reviewed a second manuscript for Monthly Weather Review.

References

Arakawa, A., and C. S. Konor, 1996: Vertical differencing of the primitive equations based on the Charney-Phillips grid in hybrid σ–p vertical coordinates. *Mon. Wea. Rev.*, **124**, 511–528, doi:10.1175/1520-0493(1996)124<0511:VDOTPE>2.0.CO;2.

CFD Direct, 2016: OpenFOAM user guide: Numerical schemes. http://cfd.direct/openfoam/user-guide/fvschemes/.

Klein, R., K. Bates, and N. Nikiforakis, 2009: Well-balanced compressible cut-cell simulation of atmospheric flow. *Phil. Trans. R. Soc. A*, **367**, 4559–4575, doi:10.1098/rsta.2009.0174.

Klemp, J. B., 2011: A terrain-following coordinate with smoothed coordinate surfaces. *Mon. Wea. Rev.*, **139**, 2163–2169, doi:dx.doi.org/10.1175/MWR-D-10-05046.1.

Lauritzen, P. H., W. C. Skamarock, M. Prather, and M. Taylor, 2012: A standard test case suite for two-dimensional linear transport on the sphere. *Geosci. Model Dev.*, **5**, 887–901, doi:10.5194/gmd-5-887-2012.

Mesinger, F., and Coauthors, 2012: An upgraded version of the Eta model. *Meteor. Atmos. Phys.*, **116**, 63–79, doi:10.1007/s00703-012-0182-z.

Schär, C., D. Leuenberger, O. Fuhrer, D. Lüthi, and C. Girard, 2002: A new terrain-following vertical coordinate formulation for atmospheric prediction models. *Mon. Wea. Rev.*, **130**, 2459–2480, doi:10.1175/1520-0493(2002)130<2459:ANTFVC>2.0.CO;2.

Shaw, J., and H. Weller, 2016: Comparison of terrain following and cut cell grids using a non-hydrostatic model. *Mon. Wea. Rev.*, **144**, 2085–2099, doi:10.1175/MWR-D-15-0226.1.

Smolarkiewicz, P. K., and J. Szmelter, 2011: A nonhydrostatic unstructured-mesh soundproof model for simulation of internal gravity waves. *Acta Geophysica*, **59**, 1109–1134, doi:10.2478/s11600-011-043-z.

Weller, H., and A. Shahrokhi, 2014: Curl free pressure gradients over orography in a solution of the fully compressible Euler equations with implicit treatment of acoustic and gravity waves. *Mon. Wea. Rev.*, **142**, 4439–4457, doi:10.1175/MWR-D-14-00054.1.

Appendices

Appendix A: Thesis plan

A new mesh for representing terrain

- Introduce existing types of mesh
- Describe the new slanted cell method

A new transport scheme for steep slopes

- Document the cubicFit transport scheme
- Two-dimensional transport tests over steep slopes
- Deformational transport tests on a spherical Earth

A generalisation of the Charney–Phillips staggering

- Describe the generalised Charney–Phillips formulation
- A nonhydrostatic model for arbitrary meshes
- A test of a quiescent atmosphere above steep slopes
- One or two tests that excite the Lorenz computational mode
- Mountain waves test case

Appendix B: Training record

Mathematics modules

Spring 2016	MA3NAT	Numerical Analysis II	unassessed
Spring 2015	MAMNSP	Numerical Solution of Partial Differential Equations	78%

RRDP modules

Summer 2017	Organising conferences
28 Feb 2017	Getting your first post-doc position
9 Nov 2016	Open Access and research data management
24 Mar 2016	Voice coaching: looking after your voice
26–27 Jan 2016	Preparing to teach (introduction, marking & feedback, leading small groups)
2 Dec 2015	An essential guide to critical academic writing
17 Nov 2015	Understanding the UK higher education context
19 May 2015	How to avoid plagiarism
10 Mar 2015	How to write a literature review
19 Feb 2015	How to write a paper

External courses

June 2016	Dynamical core intercomparison project summer school, NCAR
13 May 2016	Peer review: the nuts and bolts, Sense about Science
June 2015	Advanced numerical methods for Earth-system modelling, ECMWF

Conferences and workshops

September 2017		SciCADE, University of Bath
April 2017		PDEs on the Sphere, Paris
February 2017	Speaker	Numerical Methods for Geophysical Fluid Dynamics, Imperial College London
October 2016	Speaker	Numerical and computational methods for simulation of all-scale geophysical flows, ECMWF
July 2016	Attendee	1st GungHo Network meeting, Daresbury Laboratory
November 2015	Attendee	GungHo workshop on next generation weather and climate prediction, UK Met Office
June 2015	Attendee	Hoskins@70
June 2015	Poster	SCENARIO DTP conference
March 2015	Speaker	Galerkin methods with applications in weather and climate forecasting, ICMS

Teaching

Oct 2016	Teaching assistant	MTMW11 fluid dynamics
Oct 2015	Teaching assistant	MTMG02 atmospheric physics
Sep 2015	Teaching assistant	NCAS summer school
Sep 2014	Course teacher	MPE python and linux short course

Visits and collaborations

July 2016	Organised visit from Simon Clark, stratospheric PhD researcher and YouTube vlogger
Summer 2016	Worked with Hilary's MSc student, Christiana Skea, studying variable timestepping for ODEs
June 2016	Visited NCAR, hosted by Ram Nair
2015 – 2016	Coauthoring an article about dimensionally-split and multidimensional advection schemes, written with Hilary, her former student Yumeng Chen, and Stephen Pring at the UK Met Office

Outreach

14 Jul 2015	Schools physicist of the year awards
14 Jun 2015	East Reading festival
15 Feb 2015	Brighton science festival

Presentations

17 Nov 2016	Comp. Atmos. Dyn. group	
9 Nov 2016	PhD group	
31 Oct 2016	HHH group	
22 Sep 2016	PhD poster session	Improving numerical accuracy over steep slopes
23 Mar 2016	Quo Vadis	Numerical representation of orography in dynamical cores (honourable mention)
17 Feb 2016	PhD group	Multidimensional advection schemes for arbitrary meshes
9 Feb 2016	Mesoscale group	Curl-free pressure gradients for accurate modelling of cold air pools
19 Oct 2015	HHH group	Improving modelled mountain flows with alternative representations of terrain
27 Apr 2015	HHH group	A like-for-like comparison between terrain following and cut cell grids
21 Apr 2015	PhD group	Discrete vector calculus on Arakawa C grids
12 Feb 2015	UK Met Office	Poster presentation for Met Office Academic Partnership
18 Jan 2015	PhD group	Python and linux tips
17 Dec 2014	MPECDT jamboree	Poster presentation for Mathematics for Planet Earth Centre for Doctoral Training jamboree
12 Sep 2014	Lunchtime seminar	Gain control of your documents and code: hands-on with revision control and build automation